X-ray Analysis of Fully Depleted Thick CCDs with Small Pixels Size

I. V. Kotov[a*]for LSST camera collaboration

[a]Brookhaven National Laboratory, Upton, NY 11973, USA

ABSTRACT

^{55}Fe X-rays frames offer a lot of information about CCD characteristics. They are traditionally being used for CCD gain and charge transfer efficiency (CTE) measurements. The pixel size of modern scientific CCDs is getting smaller. The charge diffusion causes the charge spread among neighboring pixels especially in thick fully depleted sensors. This enables measurement of the charge diffusion using ^{55}Fe X-rays. On the other hand, the usual CTE characterization method based on single pixel X-ray events becomes statistically deficient. A new way of measuring CTE using shape and amplitude analysis of X-ray clusters is presented and discussed. This method requires high statistical samples. Advances in test automation and express analysis technique allows for acquiring such statistical samples in a short period of time. The details of our measurement procedure are presented. The lateral diffusion measured using e2v CCD250 is presented and implications for X-ray cluster size and expected cluster shape are discussed. The CTE analysis using total X-ray cluster amplitude is presented. This analysis can reveal CTE problems for certain conditions. The statistical analysis of average X-ray cluster shape concludes the discussion.

Keywords: CCD, charge diffusion, charge transfer efficiency, CCD X-ray detectors

1. INTRODUCTION

Specialized CCD sensors are being developed for the LSST camera. They are n-channel, fully depleted, back illuminated, $100\mu m$ thick devices with pixel size $10\mu m$. First prototypes have been produced and tested,[1].[2] For many LSST tasks achieving a small PSF is critical. Thus LSST sensors are operated in over depletion mode. The bias voltage larger than needed for full depletion is applied to the device creating the electric field up to $6kV/cm$. In thick fully depleted CCDs, charge carrier transport from the back window to the gates is accompanied by charge diffusion, for details see, for example,[3].[4] Numerous methods have been developed for lateral diffusion characterization in fully depleted Si detectors (see, for example,[5],[6],[7],[8],[9]10). These methods often require specialized equipment to perform the measurements and have sources of systematic uncertainties which are hard to eliminate. A number of these techniques have been applied to LSST prototype sensor characterization and are discussed in.[10]

We have developed a new method to obtain the characteristic diffusion σ value from analysis of the charge distribution in X-ray clusters,[11].[12] The general features of X-ray data are the following. X-ray conversions happen at all device depths. The drift time and correspondingly the diffusion sigma depend on the conversion point depth. X-ray conversions close to the gates lead to compact clusters and conversions close to the window result in wider clusters. The absorption length of 5.9 keV photons in silicon is $\approx 28.8\mu m$. For a $100\mu m$ thick device, the number of X-rays converted near the window is about 30 times higher than near the gates. Thus, the distribution of σ values in a ^{55}Fe data sample has a peak at the "window" value. The σ value for charges generated at the window surface is used to characterize the sensor's PSF. The window side PSF defines the sensor performance in the visible spectrum where photons convert in the first few microns near the window. For example, the absorption length for $400nm$ wavelength is less than $1\mu m$. It is quite practical to use ^{55}Fe X-ray data for charge diffusion characterization. Our Dewar is equipped with $10\mu Cu^{55}Fe$ source placed on the arm controlled by an actuator. The electronic driver module is outside the Dewar.

The ^{55}Fe X-ray data are routinely collected as a part of our device characterization test suite.[13] The express analysis[13] of these data reports measured gain and noise values for all CCD channels. Examples of express analysis output are shown bellow for the high statistics data set. The same data set is used to generate other

*Corresponding author, email: kotov@bnl.gov, telephone: 1 631 344-2615

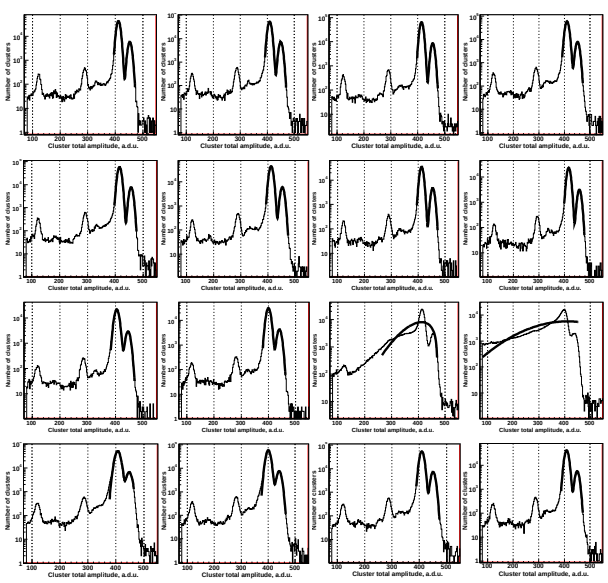

Figure 1. X-ray spectra for each CCD segment. Segment count goes from left to right and top to bottom.

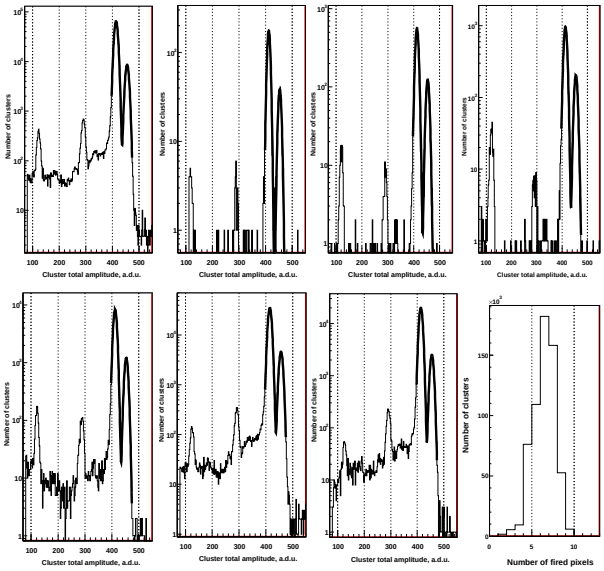

Figure 2. Segment 2 X-ray spectra for: all cluster sizes, 1, 2, 3, 4, 5 and 6 or more pixel clusters. Cluster size distribution.

plots presented in this paper. The sensor with bad segments is deliberately chosen to demonstrate analysis sensitivity and power of ^{55}Fe method in uncovering sensor defects. A ^{55}Fe run summary plots are shown in Fig.1 and an example of X-ray spectra details is shown in Fig.2 for segment 2. Black line shows $K_{\alpha,\beta}$ fit. These plots are used for gain estimation.

Segments 10 and 11 demonstrate ^{55}Fe spectra degradation. Even though $K_{\alpha,\beta}$ peaks are visible the low energy tail washes out escape and Si peaks. The cause is discussed in secsion 3.

These data are also used for the characteristic diffusion σ measurements and charge transfer efficiency (CTE) measurements as discussed bellow.

2. CHARGE DIFFUSION. MEASUREMENT METHOD AND RESULTS

The generated by X-rays initial charge cloud is very small. Initial size can be estimated from the electron range in silicon $0.012 \cdot E_\gamma^{1.75}$,[14] where E_γ is the X-ray energy in keV and range is in μm. For $5.9keV$ X-rays the range is $\sim 0.27\mu m$. During the transport from the point of generation to the gates charge cloud diffuses. The shape of diffused cloud is essentially Gaussian,[3,4] The charge sharing between neighboring pixels depends on the charge cloud size at the gates and the position of the conversion point in the pixel. The 2D Gaussian charge distribution can be described by 4 parameters: conversion point coordinates, σ, and total amplitude. These parameters can be determined for an individual X-ray if the cluster contains at least 4 pixels with amplitudes above the noise (with fewer pixels only an upper estimate on the cluster width can be obtained). The accuracy of these estimates depends on the signal to noise ratio of the cluster pixels. The low CCD noise allows for measurement of small diffusion sigmas even though the pixel size is 2-3 times larger than σ. Details of this method are presented in,[11,12] here focus is on results and their implications.

In the following example ≈6000 $K_{\alpha,\beta}$ X-ray hits and the same amount of simulated hits embedded into bias frames were analyzed. This data were obtained with CCD250 early prototype. The readout noise was $11e-$. Measured diffusion sigma values are compared with simulations as shown in Fig.3 and Fig.4. The reconstructed σ values for this data set are shown in green on both figures. They peak at $3.6\mu m$ and r.m.s. of the distribution is $0.31\mu m$. These measurements have been compared with simulations.[15] The blue histogram in Fig.3 shows reconstructed sigma values for a simulated set of 6000 $K_{\alpha,\beta}$ clusters with fixed $\sigma = 3.55\mu m$ value. Simulated X-rays are randomly distributed in x- and y-coordinates. Simulated clusters have been embedded into zero exposure images and processed through the same analysis pipeline as real ^{55}Fe frames. The data reduction algorithms are

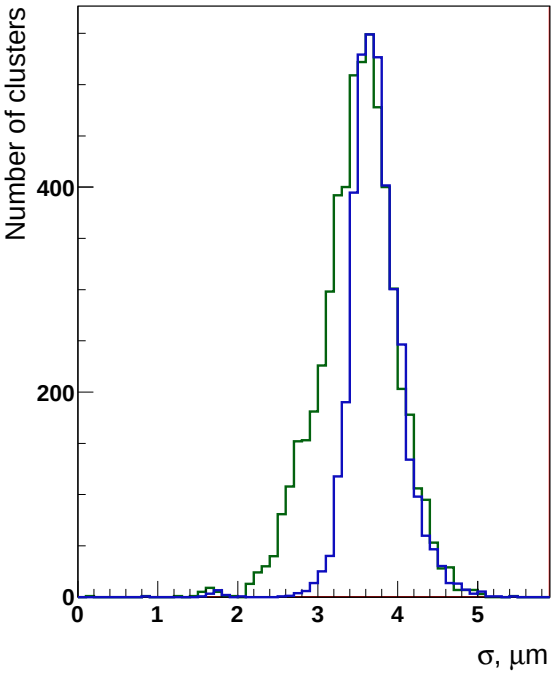

Figure 3. Measured sigma values are shown in green. The simulated X-rays with diffusion sigma value fixed at $3.55\mu m$ is shown in blue

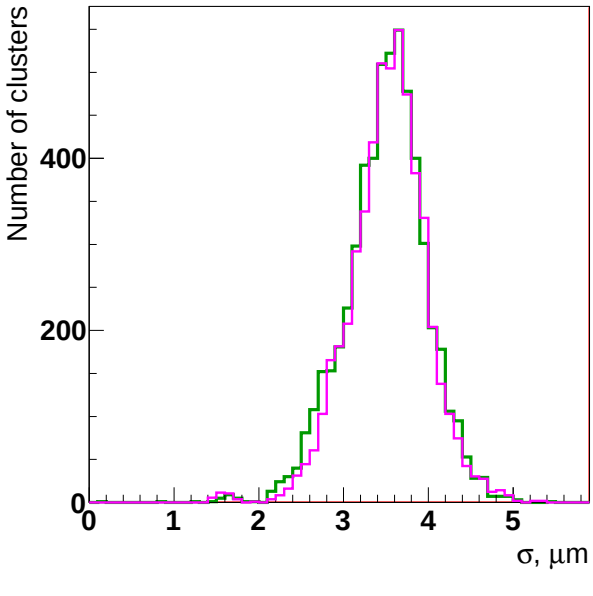

Figure 4. Measured sigma values are shown in green. The distribution obtained from simulated clusters is shown in pink.

described in,[13].[16] Measurements and simulation are in good agreement for the "window" peak. X-rays converted deeper in the bulk and away from the window, have shorter drift time and consequently smaller diffusion. These events contribute to the left of the "window" peak and have not been simulated. Thus there is a difference between green and blue histograms in this area. The characteristic diffusion value for these measurements is estimated as $\sigma = 3.55\mu m$. Should be noted this is model independent estimate and result does not depend on, for example, drift velocity knowledge.

Simulations with X-ray conversion points distributed over all depths according to X-ray absorption have been performed as well. The drift time is determined by drift velocity which in turn depends on electric field, E. The $v(E)$ parametrization[17] from measurements performed in our operating temperature range, around -100^0C, has been used. The analytical expression for E-field has be obtained solving 1D Poisson equations (following, for example[18]). Simulation results for $\sigma_{window} = 3.65\mu m$ are shown in pink in Fig.4. Both simulations are in good agreement with measurements. From these measurements, the estimated characteristic diffusion value is $\sigma = 3.6\mu m$ for our CCD.

The diffusion analysis has been performed on high statistics data set. The read out noise in this set was $\approx 7e-$. The measured σ values for first 8 channels are shown in Fig.5 and Fig.6 . The "'window"' peaks are at $3.6\mu m$ for all segments in a good agreement with early measurements. There are no segment to segment variation as expected.

The characteristic diffusion value knowledge can be used to derive general properties of X-ray clusters. Lets construct the average cluster assuming uniform distribution of X-rays along sub-pixel coordinates. This can be done analitically by convoluting 2D Gaussian cluster shape with uniform distribution in x- and y-coordinates. The average cluster shape and its variability are shown in Fig.7.

3. DEFECT DIAGNOSRICS WITH X-RAYS

X-ray spectra show low energy tails in segments 10 and 11. More information is needed to understand the cause. Such information can be obtained from the same X-ray data set. The CTE plots for segment 11, as an example,

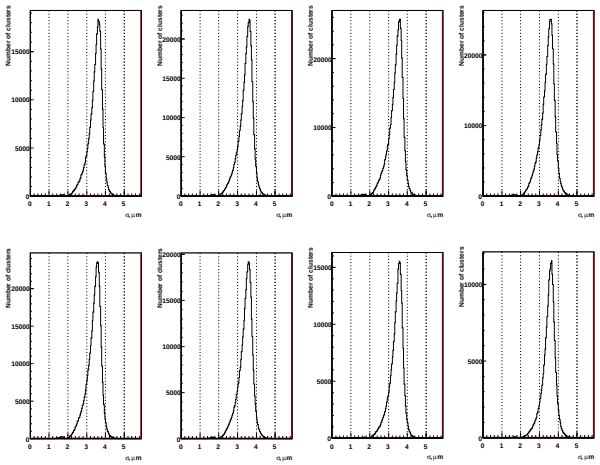

Figure 5. Measured diffusion sigma values for 8 segments.

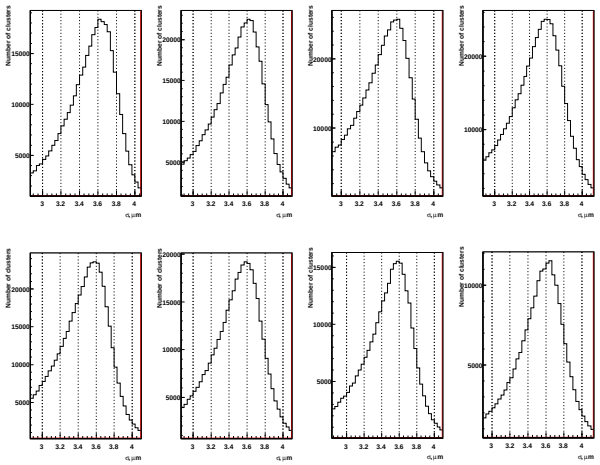

Figure 6. Same plots, zoom on the "'window"' peak.

shown in Fig.8. This figure shows that X-ray spectra are normal in some parts of this segment and are degraded in others. It is possible to pinpoint bad areas using features of the ^{55}Fe X-ray spectra itself. The largest amount of X-rays belong to K_α and K_β lines. The window framing these lines can be set and amount of events inside this window is counted depending on coordinates. The $K_{\alpha,\beta}$ count has been done in 11×20 pixel zones. In other worlds the segment area has been divided into 250 rectangular pads and $K_{\alpha,\beta}$ events have been counted in each pad. The Fig.9 shows $K_{\alpha,\beta}$ count for all segments. The areas where $K_{\alpha,\beta}$ events disappear are clearly seen in segment 10 and 11. Large amounts of traps were found in this areas using pocket pumping technique.

4. CTE MEASUREMENTS WITH X-RAYS

The diffusion spreads charges over multiple pixels and number of single pixel clusters is very limited as can be seen from Fig.2. So, using single pixel clusters for CTE measurements is not practical. From average hit properties discussed in section 2 follows that the minimal region containing on average more than 99.9% energy is 3×3 zone. This zone always contains at least 99.5% of X-ray energy. Using this zone to measure X-ray parameters is an example of aperture photometry application. Thus CTE measured using zone total amplitude is arguably a good quantity to describe the charge loss in CCD readout process. This technique has been applied to the high statistics data set. Plots illustrating CTE analysis are shown in Fig.10 for segment 2 in normal operational conditions, $T = -100^0C$. In these conditions CTE is better than 0.999999 in both serial and parallel directions. By lowering CCD temperature one can cause CTE degradation. Plots obtained at $T = -150^0C$ are shown in Fig.11 for segment 2. The CTE measured in these conditions is 0.999928 in serial direction and still better than 0.999999 in parallel direction. This corresponds to a loss of $\approx 56e-$ after 500 serial transfers and corresponding charge transfer inefficiency, CTI is $7.2 \cdot 10^{-5}$.

5. AVERAGE X-RAYS CLUSTER SHAPE AND ITS USE FOR CTE.

There is a worry that aperture CTE overestimate the CTE value. Then the central pixel, for example, might actually loose more charge then estimated using aperture CTE value. To check this we use the average pixel profile constructed both for small and large number of transfers. The construction of the profile introduced variability of the signal in the profile bins as seen in Fig.7. To measure signals for sufficient level of accuracy the averaging is needed. For example, to reach 1e- r.m.s. accuracy about 30,000 clusters are needed. There are hundreds thousands X-rays in our high statistical sample and sub electron accuracy can be reached. The average K_α clusters were constructed for data sets taken at $-100C$ and $-150C$. The number of clusters used for any segment zone was more than 200,000. Thus our accuracy level is $\approx 0.4e-$. The average clusters for normal conditions are symmetrical. The differences left-right, top-bottom are all within few sigmas. The average clusters for segment 2 at $-150C$ are shown in Table.1 and Table.2. The segment was divided into two halfs in

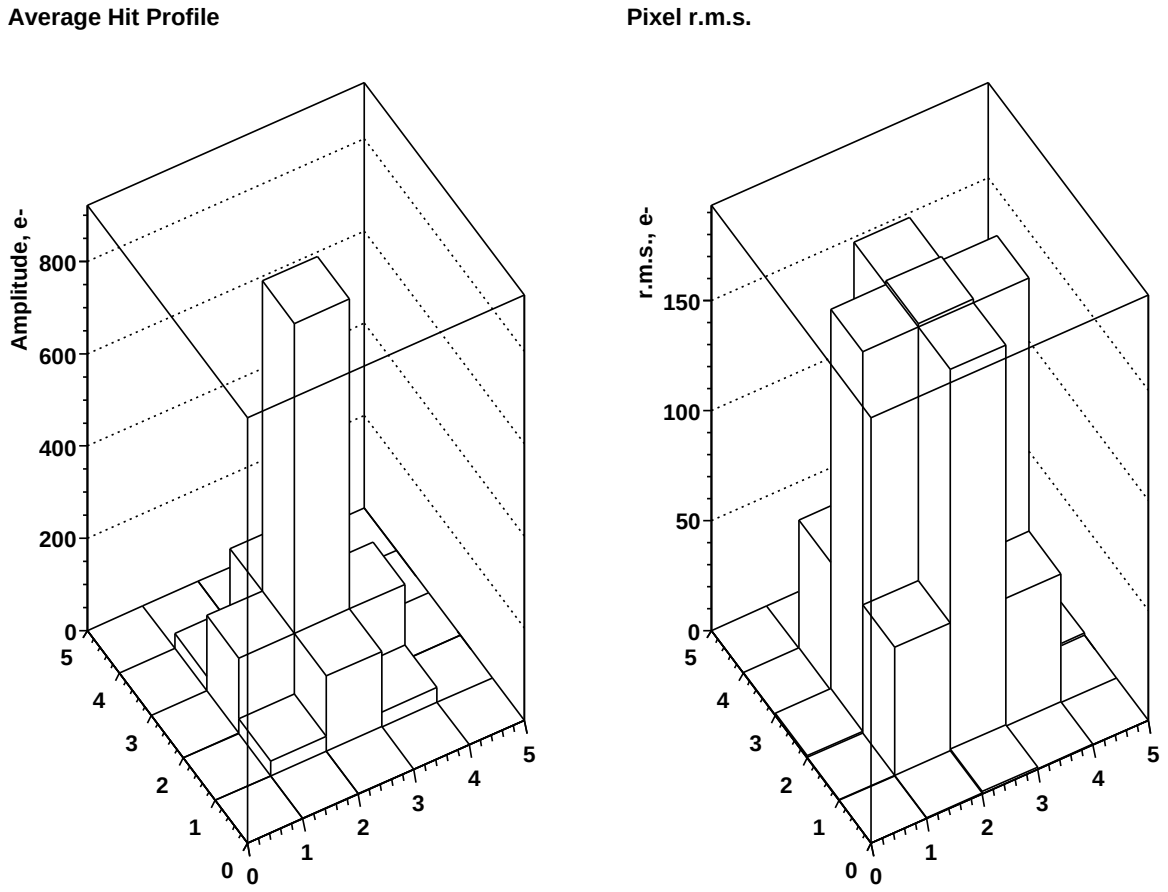

Figure 7. Average K_α hit 2D profile and variability, r.m.s., in each pixel.

Table 1. Average cluster profile close to readout node.

y/x	0	1	2
0	25.4 +/- 0.1	152.2 +/- 0.35	29.7 +/- 0.1
1	151.3 +/- 0.35	879.9 +/- 0.45	156.7 +/- 0.35
2	25.6 +/- 0.1	152.6 +/- 0.35	29.7 +/- 0.1
sum	202.3 +/- 0.4	1184.7 +/- 0.7	216.1 +/- 0.4

serial direction. Table.1 shows average cluster in the first half with number of transfers from 0 to 250 and 125 transfers on average. Table.2 shows cluster in the second half with number of transfers from 250 to 500 and 375 transfers on average. The right-left difference in the central row is $5.4e-$ in Table.1. The same difference in Table.2 is $16.4e-$. Considering the average number of transfers, 125 in the first case and 375 in the second, the excess of charges in the tail per transfer is essentially the same. Using the number of electrons in the central pixel one can calculate CTE in extended pixel response, EPER, style. This calculation gives CTE value 0.99981 and CTI is $1.9 \cdot 10^{-5}$ correspondingly. The EPER approach underestimates CTI by more than factor of 3 compare to aperture method. This is not surprising because EPER method does not take into account the release time of trapped charges. The aperture method could be refined by addition of the charge redistribution analysis within the aperture.

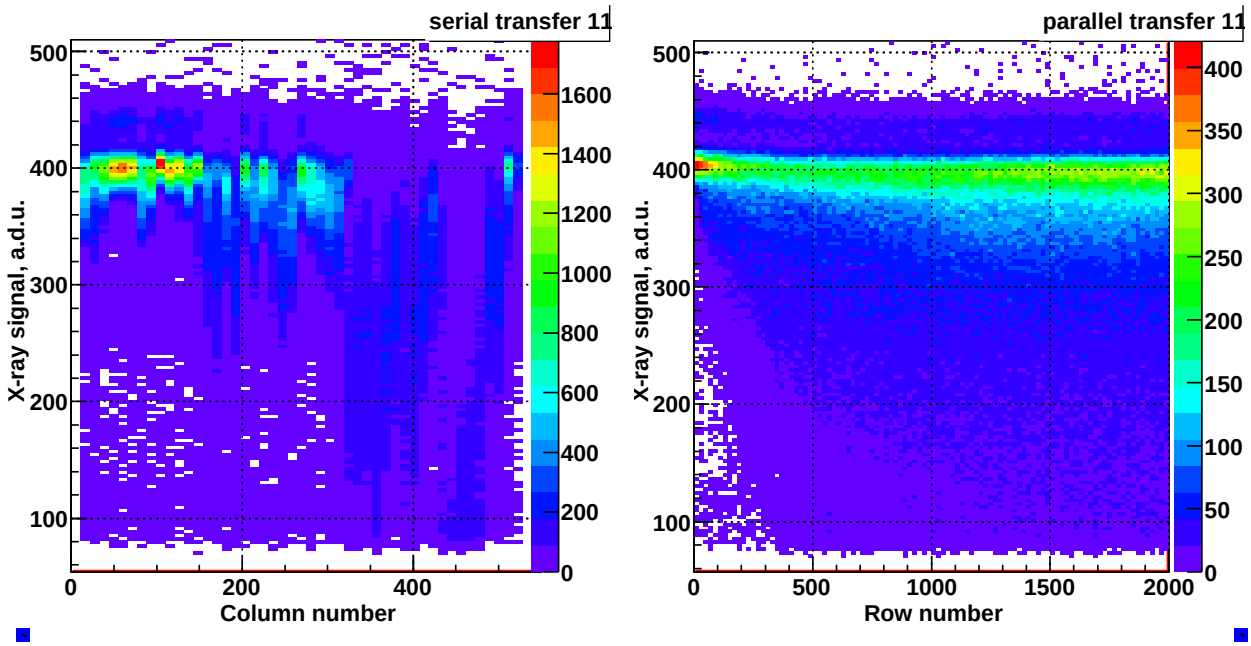

Figure 8. CTE plots for segment 11 at normal operating conditions.

Table 2. Average cluster profile away from readout node.

y/x	0	1	2
0	22.5 +/- 0.1	146.9 +/- 0.36	31.5 +/- 0.1
1	144.6 +/- 0.36	871.1 +/- 0.46	161.0 +/- 0.35
2	22.7 +/- 0.1	147.2 +/- 0.36	31.7 +/- 0.1
sum	189.8 +/- 0.4	1164.2 +/- 0.7	224.2 +/- 0.4

CONCLUSIONS

It is demonstrated that X-rays analysis is the powerful tool for CCD characterization. X-rays can be used to characterize sensor PSF for CCDs with small pixel sizes and low read-out noise. The measured on LSST prototype CCDs characteristic diffusion sigma corresponds to blue PSF value $0.17''$ (FWHM) for LSST plate scale. It is shown how X-ray analysis reveals and pinpoints defect sites. The X-rays also can be used for CTE measurements and provide practical and robust measurements.

ACKNOWLEDGMENTS

Authors acknowledge e2v technologies help in sensor prototype development.

This manuscript has been co-authored by employees of Brookhaven Science Associates, LLC.

LSST project activities are supported in part by the National Science Foundation through Governing Cooperative Agreement 0809409 managed by the Association of Universities for Research in Astronomy (AURA), and the Department of Energy under contract DE-AC02-76-SFO0515 with the SLAC National Accelerator Laboratory. Additional LSST funding comes from private donations, grants to universities, and in-kind support from LSSTC Institutional Members.

REFERENCES

1. P.O'Connor, V.Radeka, J.Frank, J.C.Geary, D.K.Gilmore, I.Kotov, P.Takacs, and J.A.Tyson, "Characterization of prototype LSST CCDs," *Proc. SPIE* **7021**, p. 702106, 2008.

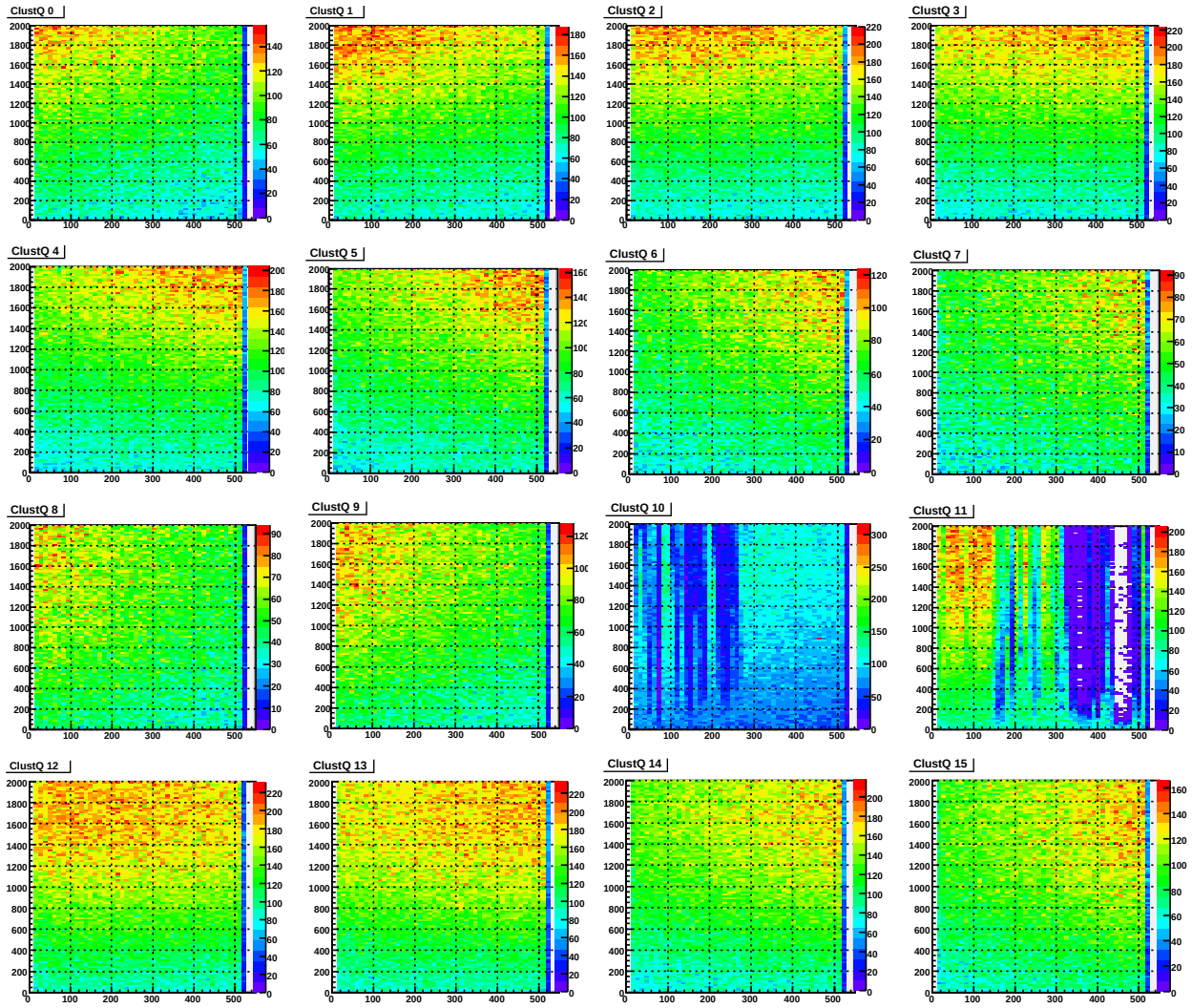

Figure 9. $K_{\alpha,\beta}$ count for all segments.

2. V.Radeka, J.Frank, J.C.Geary, D.K.Gilmore, I.Kotov, P.O'Connor, P.Takacs, and J.A.Tyson, "LSST sensor requirements and characterization of the prototype LSST CCDs," *Jinst* **4**, p. P03002, 2009.
3. J.R.Janesick, *Scientific charge-coupled devices*, vol. xvi of *SPIE Press.*, Bellingham, Wash., 2001.
4. G.G.Pavlov and J.A.Nousek, "Charge diffusion in ccd x-ray detectors," *Nuclear Inst. and Methods in Physics Research* **A428**, pp. 348–366, 1999.
5. R.Bellwied and et al, "Studies of dynamics of electron clouds in star silicon drift detectors," *Nuclear Instruments and Methods in Physics Research* **A439**, pp. 507–512, 2000.
6. H.Tsunemi, J.Hiraga, K.Yoshita, E.Miyata, and M.Ohtani, "Comparison of methods of measuring the primary charge-cloud shape produced by an x-ray photon inside the CCD," *Nuclear Instruments and Methods in Physics Research* **A439**, pp. 592–600, 2000.
7. A.Karcher and et al, "Measurement of lateral charge diffusion in thick, fully depleted, back-illuminated CCDs," *IEEE Trans. Nucl.Science* **51, No.5**, pp. 2231 – 2237, 2000.
8. S.A.Rodney and J.L.Tonry, "Characterizing charge diffusion in ccds with x-rays," *Arxiv preprint* **astro-ph/0604322**, p. arxiv.org, 2006.

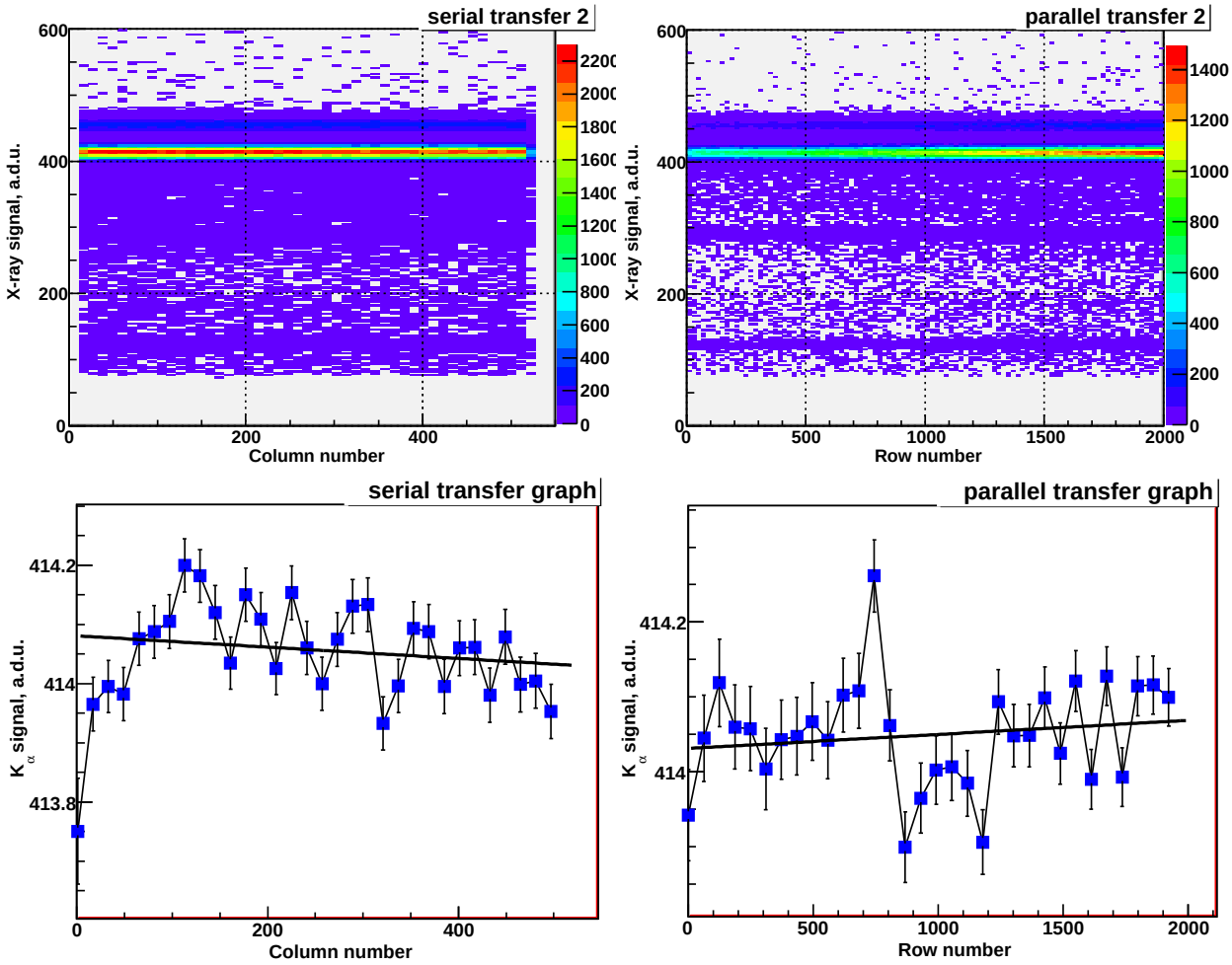

Figure 10. CTE plots for segment 2 at $T = -100^0 C$.

9. I.V.Kotov, A.I.Kotov, J.Frank, P.O'Connor, P.Kubanek, P.Takacs, and V.Radeka, "Lateral diffusion estimation in fully depleted thick CCDs using flat field image analysis," *Nuclear Inst. and Methods in Physics Research* **A652**, pp. 524–527, 2010.
10. P.Z.Takacs, I.Kotov, J.Frank, P.O'Connor, V.Radeka, and D.M.Lawrence, "Psf and mtf measurement methods for thick ccd sensor characterization," *Proc. SPIE* **7742**, p. 774207, 2010.
11. I.V.Kotov, J.Frank, A.I.Kotov, P.Kubanek, P.O'Connor, V.Radeka, and P.Takacs, "Charge diffusion measurement in fully depleted ccd using x-rays," *Nuclear Inst. and Methods in Physics Research* **A695**, pp. 296–297, 2012.
12. I.Kotov, J.Frank, A.I.Kotov, P.Kubanek, P.O'Connor, V.Radeka, and P.Z.Takacs, "Charge diffusion measurement in fully depleted ccd using 55fe x-rays," *Proc. SPIE* **8453**, p. 84531B, 2012.
13. I.V.Kotov, A.I.Kotov, J.Frank, P.Kubanek, M.Prouza, P.O'Connor, V.Radeka, and P.Takacs, "CCD characterization and measurements automation," *Nuclear Inst. and Methods in Physics Research* **A**, p. In Press, 2012.
14. T.E.Everhart and P.H.Hoff, "Determination of kilovolt electron energy dissipation vs penertation distance in solid materials," *J.Appl.Phys.* **42**, p. 5837, 1971.
15. "The C++ simulation class developed in ROOT framework is available on request from the corresponding author."
16. I.V.Kotov, A.I.Kotov, J.Frank, P.O'Connor, V.Perevoztchikov, and P.Takacs, "CCD Base Line Subtraction Algorithms," *IEEE Trans. Nucl.Science* **57, No.4**, pp. 2200 – 2204, 2010.

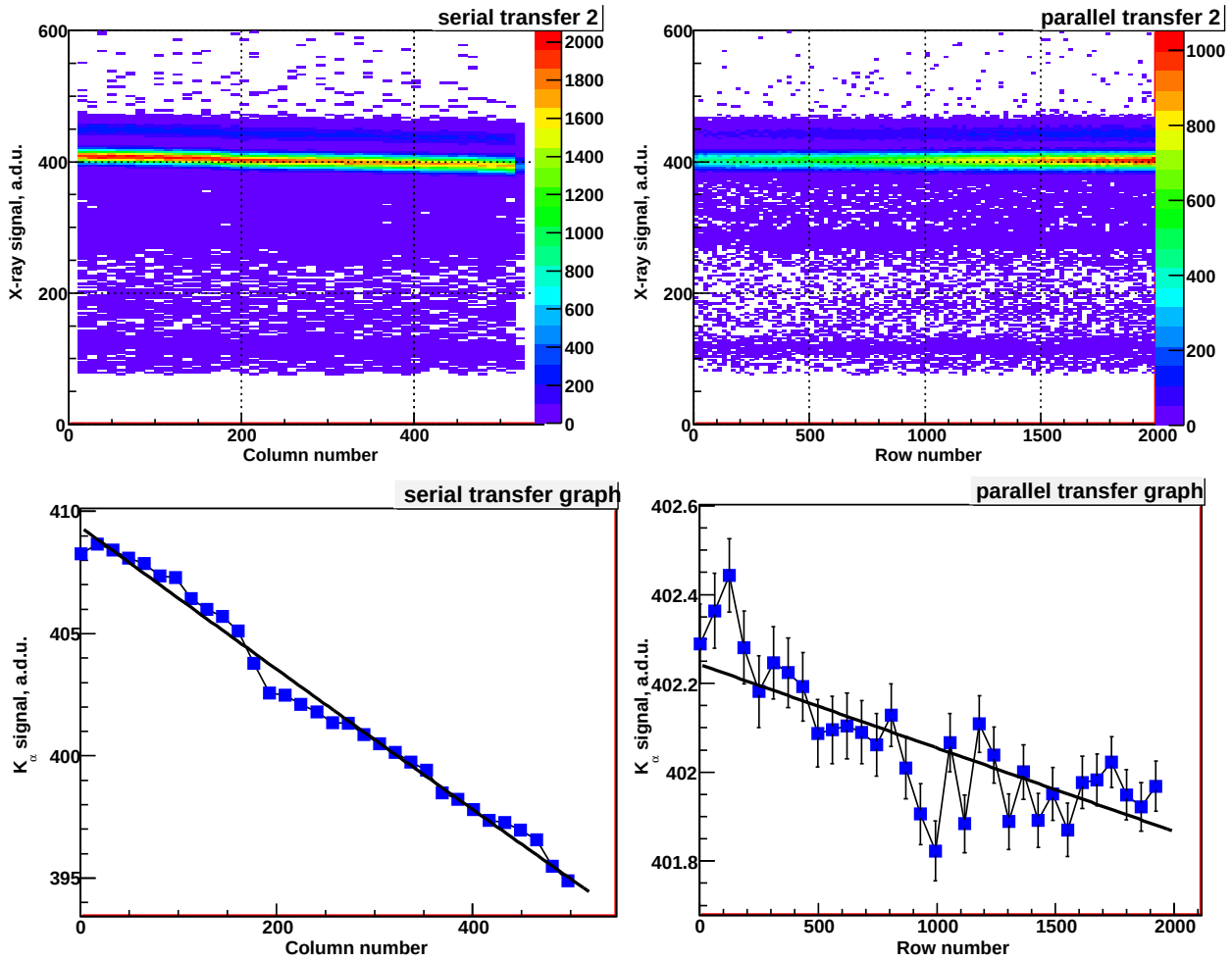

Figure 11. CTE plots for segment 2 at $T = -150^0 C$.

17. V.Eremin and Z.Li, "Carrier drift mobility study in neutron irradiated high purity silicon," *Nuclear Instruments and Methods in Physics Research* **A462**, pp. 338–343, 1995.
18. A.W.Lees and W.D.Ryan, "A simple model of a buried channel charge coupled device," *Solid-State Electronics* **17**, pp. 1163–1169, 1974.